Molecular Biology of the Cell
Vol. 20, 4531–4540, November 1, 2009

Filamin A Regulates Caveolae Internalization and Trafficking in Endothelial Cells

Maria Sverdlov,* Vasily Shinin,* Aaron T. Place,* Maricela Castellon,*† and Richard D. Minshall*†‡

Departments of *Pharmacology and †Anesthesiology and ‡Center for Lung and Vascular Biology, University of Illinois at Chicago, Chicago, IL 60612

Submitted October 6, 2008; Revised July 31, 2009; Accepted September 9, 2009
Monitoring Editor: Sean Munro

Transcytosis via caveolae is critical for maintaining vascular homeostasis by regulating the tissue delivery of macromolecules, hormones, and lipids. In the present study, we test the hypothesis that interactions between F-actin cross-linking protein filamin A and caveolin-1 facilitate the internalization and trafficking of caveolae. Small interfering RNA-mediated knockdown of filamin A, but not filamin B, reduced the uptake and transcytosis of albumin by ~35 and 60%, respectively, without altering the actin cytoskeletal structure or cell–cell adherens junctions. Mobility of both intracellular caveolin-1–green fluorescent protein (GFP)-labeled vesicles measured by fluorescence recovery after photobleaching and membrane-associated vesicles measured by total internal reflection-fluorescence microscopy was decreased in cells with reduced filamin A expression. In addition, in melanoma cells that lack filamin A (M2 cells), the majority of caveolin-1-GFP was localized on the plasma membrane, whereas in cells in which filamin A expression was reconstituted (A7 cells and M2 cells transfected with filamin A-RFP), caveolin-1-GFP was concentrated in intracellular vesicles. Filamin A association with caveolin-1 in endothelial cells was confirmed by cofractionation of these proteins in density gradients, as well as by coimmunoprecipitation. Moreover, this interaction was enhanced by Src activation, associated with increased caveolin-1 phosphorylation, and blocked by Src inhibition. Taken together, these data suggest that filamin A association with caveolin-1 promotes caveolae-mediated transport by regulating vesicle internalization, clustering, and trafficking.

INTRODUCTION

Transcytosis via caveolae is a primary mechanism of transcellular transport and thus microvascular permeability regulation (Minshall and Malik, 2006). Caveolae, in addition to functioning as signaling hubs, are thought to be important for shuttling plasma albumin, insulin, steroid hormones, and other molecules that bind to albumin from blood to tissues (Minshall *et al*., 2003; Hu *et al*., 2008a). Increased transport through pulmonary microvessel endothelial cells via caveolae was found to play a causal role in inflammatory vascular hyperpermeability (Hu *et al*., 2008b). However, the underlying molecular mechanisms that regulate caveolae trafficking in endothelial cells are poorly defined (Parkar *et al*., 2009). Thus, a better understanding of the cellular processes regulating caveolae trafficking should provide novel therapeutic strategies for preventing protein-rich edema formation and targeting the delivery of drugs.

This article was published online ahead of print in *MBC in Press* (http://www.molbiolcell.org/cgi/doi/10.1091/mbc.E08–10–0997) on September 16, 2009.

Address correspondence to: Richard D. Minshall (rminsh@uic.edu).

Abbreviations used: BSA, bovine serum albumin; Cav-1, caveolin-1; CTB, cholera toxin subunit B; DAPI, 4,6-diamidino-2-phenylindole; FLN, filamin; FRAP, fluorescence recovery after photobleaching; GFP, green fluorescent protein; HMVEC, human microvascular endothelial cell(s); Lat B, latrinculin B; PP2, 4-Amino-5-(4-chlorophenyl)-7-(t-butyl)pyrazolo[3,4-d]pyrimidine; TIR-FM, total internal reflection fluorescence microscopy; WT, wild type; YFP, yellow fluorescent protein.

Although electron micrographs suggest the majority of caveolae are linked to submembranous actin filaments (Izumi *et al*., 1991; Morone *et al*., 2006; Richter *et al*., 2008), the role of the cytoskeleton in caveolae-mediated endocytosis and transcytosis is not clear. Disruption of the actin cytoskeleton was shown not only to block uptake of cross-linked alkaline phosphatase localized to caveolae (Parton *et al*., 1994) but also to promote internalization of green fluorescent (GFP)–caveolin-1-labeled vesicles (Mundy *et al*., 2002). Increased lateral migration and clustering of otherwise stable caveolae at the plasma membrane was also observed upon depolymerization of actin filaments (Pelkmans *et al*., 2002; Thomsen *et al*., 2002). According to the model developed by Pelkmans *et al*. for caveolae-mediated internalization of simian virus 40, entrapment of viral particles in caveolae induces a tyrosine phosphorylation cascade followed by local disassembly of the cortical actin cytoskeleton and actin polymerization around loaded caveolae (Pelkmans and Helenius, 2002; Pelkmans *et al*., 2002). Thus, the actin cytoskeleton seems to play a dual role in caveolae internalization: first, it organizes caveolae at the plasma membrane and restricts their lateral movement; and second, it is necessary for efficient vesicle budding and detachment from the membrane.

The large GTPase dynamin-2, which is recruited to the neck of caveolae upon cargo loading and caveolin-1 phosphorylation (Shajahan *et al*., 2004a) has an ability to organize the actin cytoskeleton and regulate actin tail formation (Lee and Camilli, 2002; Orth *et al*., 2002). One possibility is that dynamin-2 mediates its effect on actin through cortactin, which was shown to bind dynamin-2 both in vivo and in vitro (McNiven *et al*., 2000; Schafer *et al*., 2002; Krueger *et al*.,

2003). Another dynamin binding partner, intersectin, promotes actin polymerization by activating Wiskott–Aldrich syndrome protein and thereby is thought to regulate caveolae fission from the membrane (Predescu *et al*., 2003).

Caveolin-1, the primary structural protein of caveolae, was shown to bind actin cross-linking proteins filamin (FLN) A and filamin B in vitro and in vivo (Stahlut and van Deurs, 2000). Recent data confirmed that filamin A forms a complex with caveolin-1 in different cell systems (Doucey *et al*., 2006; Head *et al*., 2006; Ravid *et al*., 2008b). Functions assigned to this interaction include activation of the actin-folding and chaperone protein T-complex protein-1, which is normally inhibited by caveolin-1 (Doucey *et al*., 2006), and stimulation of Akt-dependent phosphorylation of filamin A, which inhibits calpain-mediated cleavage of filamin A (Ravid *et al*., 2008a). In addition to organization of the actin cytoskeleton, filamin A was shown previously to regulate signal transduction (Stossel *et al*., 2001) and control receptor trafficking (Onoprishvili *et al*., 2003; Seck *et al*., 2003; Beekman *et al*., 2008). In the present study, we tested the hypothesis that filamin A regulates caveolae-mediated endocytosis and trafficking by providing a link between caveolin-1 and the actin cytoskeleton.

MATERIALS AND METHODS

Cell Culture

Human lung microvascular endothelial cells (HLMVECs) (Lonza Walkersville, Walkersville, MD) were cultured on dishes coated with 0.2% gelatin in endothelial basal media-2-MV (Lonza Walkerville) supplemented with 20% fetal bovine serum (FBS), L-glutamine, 50 U/ml penicillin, and 50 μg/ml streptomycin. M2 and A7 melanoma cell lines, kindly provided by Dr. F. Nakamura (Brigham and Women's Hospital, Harvard Medical School, Boston, MA), were grown in minimal essential medium (Invitrogen, Carlsbad, CA) supplemented with 10% FBS, 10 mM HEPES, 50 U/ml penicillin, and 50 μg/ml streptomycin. A7 media also contained 50 μg/ml G418 (Invitrogen).

Mouse lung microvascular endothelial cells (MLMVECs) from wild-type (B6/129SJ2) and caveolin-1 null mice of the same genetic background (The Jackson Laboratory, Bar Harbor, ME) were isolated and maintained in culture by using an original set of methods (Shinin *et al*., unpublished data). In brief, isolated perfused lung lobes were partially digested in freshly prepared collagenase type 1 (Sigma-Aldrich, St. Louis, MO) solution in DMEM (high glucose; Invitrogen) and gently dissociated. Peripheral lung fragments devoid of large-diameter vessels, conductive airways, and surrounding connective tissue were collected and observed to be enriched in bronchiolo-alveolar units containing microvasculature networks. These distal lung fragments were washed and further digested in mild trypsin solution (Invitrogen) to obtain a single-cell suspension. Cells were plated at the density of 2000–10,000 cells/cm^2 on Matrigel-coated dishes and kept in endothelial cell growth medium (DMEM/Ham's F-12 base + 10% fetal calf serum (HyClone Laboratories, Logan, UT), 50 μg/ml endothelial cell growth supplement (Sigma-Aldrich), and 20 ng/ml vascular endothelial growth factor for ~3 wk. Endothelial cell colonies (usually 3–5/dish) individually grown as secondary cultures were then characterized by immunostaining. These cultures where 100% positive for platelet endothelial cell adhesion molecule-1 (CD31), VE-cadherin, Flk-1, and von Willebrand factor but did not exhibit prominent α-smooth muscle actin–positive stress fibers or cytokeratins and thus judged to be pure endothelial cell cultures.

Reagents

All reagents were obtained from Sigma-Aldrich unless stated otherwise. 4-Amino-5-(4-chlorophenyl)-7-(*t*-butyl)pyrazolo[3,4-*d*]pyrimidine (PP2), latrinculin B (Lat B), and jasplakinolide were obtained from Calbiochem (San Diego, CA). Filamin A monoclonal antibody (Ab) and filamin B polyclonal Ab were obtained from Millipore Bioscience Research Reagents (Temecula, CA). Caveolin-1 polyclonal Ab, pY14-caveolin-1 monoclonal antibody (mAb), caveolin-2 mAb, dynamin-2 mAb, flotillin-1 mAb, and early endosome antigen (EEA)1 mAb were from BD Biosciences (San Jose, CA). Monoclonal antibodies for β-actin, FLAG-tag, and vimentin were from Sigma-Aldrich. c-Src polyclonal Ab and normal mouse immunoglobulin G (IgG) were obtained from Santa Cruz Biotechnology, (Santa Cruz, CA). 4,6-Diamidino-2-phenylindole (DAPI), Alexa-488 bovine serum albumin (BSA), Alexa-546 cholera toxin subunit B (CTB), Alexa-568 phalloidin, and all fluorescently labeled secondary antibodies were purchased from Invitrogen. Horseradish peroxidase-conjugated goat-anti-mouse and goat-anti-rabbit secondary antibodies were from Kirkegaard and Perry Laboratories (Gaithersburg, MD). *n*-Octylglucoside and ATP were purchased from Research Products International (Mt. Prospect, IL).

cDNA Cloning and Transfection

Full-length *Homo sapiens* filamin A-red fluorescent protein (RFP) was a gift from Dr. F. Nakamura (Brigham and Women's Hospital). The C-terminal fragments of filamin A in pQE30 vector pQE30-FLN A 22-24, pQE30-FLN A 22-23h, and pQE30-FLN A 22-23 were kindly provided by Dr. W. H. Ziegler (Technical University Carolo-Wilhemina at Brunswick, Brunswick, Germany). Fragments were recloned into pRK5 vector (BD Biosciences) by using BamHI and HindIII restriction sites. Actin-yellow fluorescent protein (YFP) was a gift from Dr. D. Mehta (University of Illinois, Chicago, IL). Full-length *H. sapiens* caveolin-1 was used as a template to generate C-terminal GFP-tagged caveolin-1 (Cav-1-GFP). The primer pair Cav-1-NheI-F: 5′-ACT-AGCTAGCGGCCACCATGTCTGGGGGCAAATAC-3′ and Cav-1-KpnI-R: 5′-ACTGGGTACCGTTATTTCTTTCTGCAAGTTGATGCG-3′ was used to generate caveolin-1 that lacks the stop codon. The resulting polymerase chain reaction (PCR) fragment was digested with restriction enzymes NheI and KpnI (Invitrogen) and subcloned into pEGFP-N1 vector (Clontech, Mountain View, CA).

HLMVECs were transfected with filamin A C-terminal fragments, actin-YFP, or Cav-1-GFP alone or in combination with control, FLN A, or FLN B small interfering RNA (siRNA) by Nucleofector (Amaxa Biosystems, Gaithersburg, MD) according to the manufacturer's instructions. Cells were used for experiments 48 h after cDNA transfection or 72 h after cDNA and siRNA cotransfection.

M2 and A7 cells were transfected with Cav-1-GFP and filamin A-RFP by Nucleofector. Twenty-four hours after transfection, cells were fixed, stained with filamin A mAb, and analyzed by confocal microscopy using an LSM 510 META confocal microscope (Carl Zeiss MicroImaging, Thornwood, NY).

Fractionation by Density Gradient Centrifugation

Fractionation was conducted as described previously (Macdonald and Pike, 2005) with slight modifications. For stimulation experiments, cells were starved for 3 h and incubated with sodium orthovanadate (10 μM) for 15 min followed by stimulation with 30 mg/ml BSA (fraction V, 99% pure, endotoxin free) for 15 min. In brief, two confluent 10-cm plates were washed and scraped into base buffer (20 mM Tris-HCl, pH 7.8, and 250 mM sucrose) supplemented with 1 mM $CaCl_2$ and 1 mM $MgCl_2$. Cells were centrifuged at 1000 $\times$ *g* for 10 min, and the cell pellet was resuspended in 1 ml of base buffer containing 1 mM $CaCl_2$, 1 mM $MgCl_2$, and protease inhibitor cocktail (Sigma-Aldrich). Cells were lysed by 40 strokes in Dounce homogenizer followed by passage through a 27-gauge needle 10 times. Lysates were centrifuged at 10,000 $\times$ *g* for 10 min to remove unbroken cells and large cell fragments. Supernatants were collected and mixed with an equal volume of 50% OptiPrep and overlaid with 20, 15, 10, 5, and 0% OptiPrep gradient in base buffer containing 1 mM sodium orthovanadate. Gradients were centrifuged at 52,000 $\times$ *g* in SW55Ti rotor for 10 h at 4°C. Twelve fractions were collected starting from the top of the gradient and equal volume samples of each fraction were analyzed by SDS-polyacrylamide gel electrophoresis (PAGE).

Immunoprecipitation and Western Blot Analysis

For stimulation studies, cells were starved for 3 h and then pretreated with sodium orthovanadate (10 μM for 15 min), PP2 (10 μM for 15 min), and/or BSA (30 mg/ml for 15 min). For Western blotting, cells were lysed on ice for 30 min in lysis buffer containing 20 mM Tris-HCl, pH 7.4, 150 mM NaCl, 1 mM EDTA, 60 mM *n*-octylglucoside, 1% Triton X-100, 1 mM phenylmethylsulfonyl fluoride, 1 mM sodium orthovanadate, and protease inhibitor cocktail. All insoluble materials were removed by centrifugation (100,000 $\times$ *g* for 45 min). For immunoprecipitations, lysates were incubated with M-280 Dynabeads coated with sheep anti-mouse IgG (Invitrogen) preconjugated with monoclonal anti-filamin A or anti-FLAG antibodies for 1 h at 4°C. Proteins were resolved by SDS-PAGE, processed with an enhanced chemiluminescence SuperSignal kit (Pierce Chemical, Rockford, IL), and then the relative band intensities (densitometry) from scanned blots determined using ImageJ software (National Institutes of Health, Bethesda, MD).

siRNA Transfection

FLN A, FLN B, and Cav-1 siRNA ON-TARGETplus Smart pools were purchased from Dharmacon RNA Technologies (Lafayette, CO). siGENOME Nontargeting pool #1 (Dharmacon RNA Technologies) was used as a control. HLMVECs grown to 80–90% confluence were transfected with 50 nM pooled siRNA by using DharmaFECT I (Dharmacon RNA Technologies) according to the manufacturer's instructions. Cells were used for experiments 72 h after transfection. The level of knockdown was quantified by densitometric analysis of Western blots by using ImageJ software.

Fluorescent Albumin Uptake, Immunostaining, and Confocal Microscopy

For uptake experiments, confluent HLMVECs grown on collagen-coated glass coverslips or MLMVECs purified from wild-type (WT) or caveolin-1 null

(*Cav1*$^{-/-}$) mice grown on Matrigel-coated coverslips were starved for 5 h in basal media and incubated with Alexa-488-BSA (10 μg/ml) in basal media containing 0.1 mg/ml unlabeled BSA for 30 min at 37°C. Cells were washed with acid wash buffer, pH 2.5, and Hanks' balanced salt solution to remove surface-bound BSA; fixed with 4% paraformaldehyde (PFA); permeabilized with 0.1% Triton X-100; and stained with FLN A, FLN B, or Cav-1 antibodies and the nuclear marker DAPI (1 μg/ml). For quantification of uptake in siRNA-transfected or Lat B (25 nM for 20 min)-pretreated cells, 10 images of equal area were taken per sample, and each experiment was repeated three times. Alexa-488-BSA uptake was estimated from thresholded images by using the ImageJ Particle Analysis module.

For immunostaining, confluent serum-grown HLMVECs were fixed with 4% PFA, permeabilized, and incubated with FLN A or FLN B antibodies (1 μg/ml). Nonconfocal DAPI images were acquired using mercury lamp excitation and UV filter set. Confocal microscopy was performed using an LSM 510 META microscope (Carl Zeiss MicroImaging) with 488- and 543-excitation laser lines and pinhole set to achieve 1 Airy unit. Z-axis orthogonal projections of M2 and A7 cells transfected with Cav-1-GFP and FLN A-RFP were obtained by processing confocal slices collected in 0.34-μm step increments using the LSM 510 META 2D deconvolution module.

^{125}I-Albumin Transendothelial Transport

Transcellular ^{125}I-albumin permeability of HLMVEC monolayers transfected with control (nontargeting), FLN A, FLN B, or Cav-1 siRNA was calculated as described previously (John *et al*., 2003; Shajahan *et al*., 2004b). For permeability studies, cells were grown on 12-mm-diameter polyester Transwell membranes with 0.4-μm pore size (Corning Life Sciences, Lowell, MA) coated with collagen and starved for 5 h before each experiment. ^{125}I-Albumin in the presence of 0.1 or 100 mg/ml unlabeled albumin was added to the upper chamber, and aliquots were collected from the lower chamber (which also contained an equal amount of unlabeled albumin) at 20, 40, and 60 min. ^{125}I-Albumin transport was measured in triplicate and repeated three times. Specific vesicular ^{125}I-albumin permeability (that which was displaced by excess unlabeled albumin) was calculated for each time point as described previously (John *et al*., 2003).

F/G-Actin Fractionation

F/G-actin fractionation was performed as described previously (Searles *et al*., 2004). In brief, confluent HLMVECs were lysed in a buffer containing 50 mM piperazine-*N*,*N*′-bis(2-ethanesulfonic acid), pH 6.9, 50 mM NaCl, 5 mM $MgCl_2$, 5 mM EGTA, 5% glycerol, 0.1% Nonidet P-40, 0.1% Triton X-100, 0.1% Tween 20, 1 mM ATP, and protease inhibitor cocktail, and lysates were centrifuged at 100,000 $\times$ *g* for 1 h at 37°C. The supernatant (G-actin fraction) was saved and the cell pellet (F-actin fraction) was incubated with 1 μM cytochalasin D in ice-cold distilled H_2O for 1 h. G-actin and F-actin levels were determined from equal volume aliquots from each fractions by Western blot analysis using anti-actin mAb. The ratio of G-actin to F-actin was quantified by scanning densitometry. Lysates from HLMVECs incubated with 100 nM latrinculin B for 30 min or with 100 nM jasplakinolide for 30 min were used as controls.

Fluorescence Recovery after Photobleaching (FRAP)

HLMVECs were cotransfected with Cav-1-GFP and siRNA and grown on glass-bottom collagen-coated dishes for 48 h. Live-cell confocal imaging was performed at 37°C with an LSM 510 META system (Carl Zeiss MicroImaging) by using a 63 $\times$ 1.45 numerical aperture (NA) H_2O-immersion lens. A small intracellular region was bleached with the 488-nm laser line set to full power for 30 iterations. Recovery of fluorescence was monitored for 20 cycles with a time lapse of 16.6 s with reduced laser power (1% transmission). Images were processed with LSM 510 META software. Relative intensity (RI) was calculated from the following equation: RI = It(0)/Ib(0) $\times$ Ib(t)/It(t), where It(0) is the total intensity of the cell before bleaching, Ib(0) is the intensity of the bleached area before bleaching, Ib(t) is the intensity of the bleached area after bleaching at time *t*, and It(t) is the intensity of the whole cell after bleaching at time *t*. The rate of fluorescence recovery was calculated from the slope of the linear region of the recovery curve immediately after photobleaching.

Total Internal Reflection-Fluorescence Microscopy (TIR-FM) Imaging and Quantification

HLMVECs were cotransfected with Cav-1-GFP and control or FLN A siRNA and plated onto gelatin-coated glass-bottomed dishes (MatTek, Ashland, MA). Seventy-two hours after transfection, cells were subjected to TIR-FM analysis using an Axio Observer Z1 inverted microscope equipped with Dynamic Laser TIR-FM module (Carl Zeiss MicroImaging) and ORCA-II ERG charge-coupled device camera (Hamamatsu, Bridgewater, NJ). Dynamics of Cav-1-GFP were acquired with a 100×/1.45 NA alpha Plan Fluar oil immersion objective at 37°C. Thirty frame recordings (0.9-s exposure per frame) were collected and processed using the Delta-F-up ImageJ plug-in to subtract each image in the stack from the preceding image, and then Z-projections over time of the subtracted stacks were created. Dynamic events, which included all movement of Cav-1-GFP in the total internal reflectance fluorescence (TIRF) plane, were quantified from thresholded Z-projections for control siRNA and FLN A siRNA-transfected cells (16 cells/group, 3–4 areas/cell) using the ImageJ Particle Analysis plug-in. For quantification, areas free of large fluorescent aggregates of Cav-1-GFP were selected. Results are presented as the percentage of the number of events detected in the TIRF plane over 30 frames per unit area.

Statistical Analysis

Statistical comparisons of albumin uptake and transendothelial transport results were conducted using ANOVA with significance level set at $p < 0.05$. Statistical significance of FRAP and TIR-FM results were estimated by nonpaired Student's *t* test.

RESULTS

FLN A Associates with Caveolin-1 in Endothelial Cells and Partially Localizes to Buoyant Density Gradient Fractions

To determine whether FLN A associates with Cav-1 in endothelial cells, we immunoprecipitated Cav-1 from whole cell lysates and blotted for FLN A and FLN B. In the absence of a specific stimulus, a small amount of FLN A, but not its homologue FLN B, coprecipitated with Cav-1 (Figure 1A). These results suggest that under basal conditions, a fraction of FLN A is associated with Cav-1 in endothelial cells.

In vitro studies previously localized the FLN A Cav-1 binding site to its C terminus (Stahlut and van Deurs, 2000). To confirm the association between FLN A and Cav-1, HLMVECs were transfected with FLAG-tagged C-terminal fragments of FLN A containing domains 22-23 (FLN 22-23), domains 22-23, and the hinge region (FLN 22-23h), and domains 22-24 (FLN 22-24). FLN A fragments were then immunoprecipitated from whole cell lysates, separated by SDS-PAGE, transferred, and blotted for FLN A and Cav-1 (Figure 1B). Only the complete C terminus of FLN A, containing domains 22-24, was able to coimmunoprecipitate Cav-1 (Figure 1B).

To detect whether FLN A associates with caveolae in endothelial cells, we subjected HLMVEC lysates to centrifugation in OptiPrep gradients. Fractions 1 through 4 collected from the top of the gradient were shown to be enriched in cholesterol (Macdonald and Pike, 2005) and are representative of lipid rafts (Figure 1C). These fractions also contained a large amount of flotillin-1, an established marker of lipid rafts, as well as Cav-1, Cav-2, and c-Src kinase. A second peak of flotillin-1, Cav-1, and Cav-2 occurred in fractions 6 through 8. These fractions have a moderate amount of cholesterol; thus, it is possible that they represent a subset of caveolae. Another possibility is that lipid raft markers that occur in these fractions are localized in the Golgi. Finally, the last four fractions (9–12) contained the majority of cytoskeletal and cytosolic proteins not associated with lipids.

We propose fractions 1–4 represent caveolae actively participating in endocytosis because both Src and dynamin-2, which are required for fission of caveolae from the membrane, partially localize to these fractions but not to fractions 6 through 8. We also detected a small amount of actin and FLN A in fractions 2 and 3 in nonstimulated cells.

Filamin A–Caveolin-1 Interaction Is Promoted by the Activation of Caveolae-mediated Endocytosis

To assess the role of FLN A–Cav-1 interactions in caveolae-mediated transport in endothelial cells, we compared the amount of Cav-1 coimmunoprecipitated with FLN A from lysates of starved cells and cells in which caveolae-mediated endocytosis was activated by addition of BSA (John *et al*., 2003; Shajahan *et al*., 2004a). Cav-1 association with FLN A

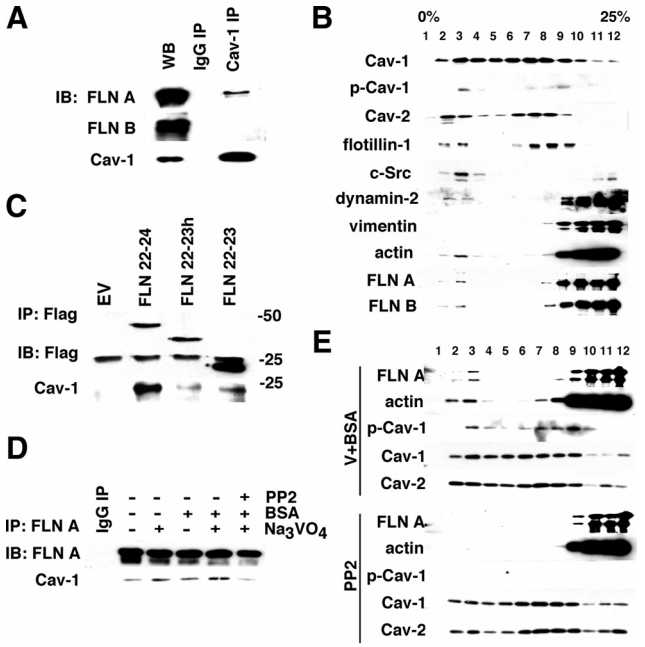

Figure 1. Src regulation caveolin-1–filamin A interaction and lipid raft association. (A) HLMVECs grown in complete media were lysed, and clarified whole cell lysates were used for caveolin-1 immunoprecipitation. Western Blot analysis indicates that a small fraction of FLN A but not its homologue FLN B associates with Cav-1. (B) Fractionation by centrifugation in density gradients. HLMVECs grown in complete medium were mechanically disrupted in detergent-free buffer and subjected to fractionation in 0–25% OptiPrep gradients. Twelve fractions were collected starting from the top of the gradient and analyzed by Western blotting. Cav-1, Cav-2, and lipid raft marker flotillin-1 showed a similar biphasic distribution with peaks in fractions 2 and 3 and fractions 6–8. c-Src was primarily localized to cholesterol-enriched fractions (1–3), whereas vimentin and the majority of cytosolic- and cytoskeletal-associated proteins were concentrated in the heavier fractions (9–12). A small amount of dynamin-2, actin, and FLN A were found in the Cav-1–positive cholesterol-enriched fractions (fractions 2 and 3), suggesting that these proteins might be associated with caveolae. (C) FLAG-tagged C-terminal fragments of human FLN A, containing domains 22-23 (FLN 22-23), domains 22-23, and the hinge region (FLN 22-23h), and domains 22-24 (FLN 22-24) were expressed in HLMVECs. Cells were lysed and constructs were immunoprecipitated from the whole cell lysate. Western blot results suggest that Cav-1 binds primarily the complete C-terminal fragment containing domains 22-24. (D) HLMVECs were starved and incubated with BSA (30 mg/ml for 15 min), sodium orthovanadate (10 μM for 15 min), and Src kinase inhibitor PP2 (10 μM for 30 min) alone or in combination. FLN A was immunoprecipitated from the whole cell lysate, and the amount of Cav-1 coprecipitated with FLN A was analyzed by Western blot. Incubation with both BSA and sodium orthovanadate increased the coprecipitation of FLN A and Cav-1, whereas pretreatment with PP2 prevented this increase in association. (E) Starved HLMVECs were incubated with a mixture of sodium orthovanadate and BSA or PP2 as described in D. Lysates were subjected to fractionation in the density gradient and fractions were analyzed by Western blotting with antibodies against FLN A, actin, Cav-1, phospho-caveolin-1 (pY14-Cav-1), and Cav-2. Cells treated with sodium orthovanadate and BSA showed increased amount of pY14-Cav-1 as well as a shift of FLN A and actin to cholesterol-enriched fractions, thus leading to the higher degree of cofractionation of Cav-1 with FLN A and actin. In cells pretreated with PP2, Cav-1 phosphorylation induced by BSA and sodium orthovanadate was blocked, and the amount of both FLN A and actin in buoyant fractions was significantly reduced.

was increased after stimulation with BSA compared with starved cells (Figure 1D). Cotreatment with sodium orthovanadate, a general inhibitor of tyrosine phosphatases previously shown to stimulate caveolae internalization (Shajahan *et al*., 2004a), induced a further increase in the association of Cav-1 and FLN A. This effect was significantly blocked by PP2, an inhibitor of Src-family kinases shown previously to block Cav-1 phosphorylation and caveolae-mediated endocytosis (Shajahan *et al*., 2004a).

We also compared the distribution of actin and FLN A in gradient fractions from HLMVECs under basal conditions and after activation of caveolae-mediated endocytosis. Addition of BSA and sodium orthovanadate induced an increase in Cav-1 phosphorylation and shift of both FLN A and actin to fractions 2 and 3 (Figure 1E), suggesting that FLN A and actin are recruited to loaded and activated caveolae. Preincubation of cells with PP2 decreased the amount of FLN A and actin in buoyant fractions of the gradient. Taken together, these results imply that upon cargo loading and activation of caveolae internalization, FLN A and actin are recruited to caveolae and interact with Cav-1.

siRNA-mediated Knockdown of filamin A, but Not of Filamin B, Reduces Albumin Uptake in HLMVECs

The importance of FLN A in caveolae-mediated endocytosis was addressed by knocking down FLN A with siRNA. siRNA for its homologue FLN B and for Cav-1 itself were used as controls in these experiments. FLN A, FLN B, and Cav-1 siRNA were specific and did not affect the expression levels of each other, tubulin, or glyceraldehyde-3-phosphate dehydrogenase as assessed by Western blot analysis (Figure 2A). siRNA transfection reduced protein expression level by 76% for FLN A, by 82% for FLN B, and by 67% for Cav-1 as quantified by densitometry of Western blots (Supplemental Figure S1A).

To measure the ability of HLMVEC transfected with FLN A and FLN B siRNA to internalize albumin, starved cells were incubated with Alexa-488-BSA for 30 min. As shown in Figure 2B, we observed a decrease in albumin endocytosis in cells transfected with siRNA for FLN A, but not in cells transfected with control siRNA or FLN B siRNA. Cells transfected with siRNA for the main structural protein of caveolae, Cav-1, or a mixture of siRNA for FLN A and Cav-1, showed a similar decrease in albumin uptake. Finally, pretreatment with 25 nM latrinculin B for 20 min induced a significant reduction in albumin internalization (Figure 2B). Uptake was quantified from multiple thresholded images of equal area from three separate experiments (Figure 2C). siRNA-mediated knockdown of FLN A and Cav-1 induced a 35 and 41% reduction in BSA uptake respectively, whereas reduction in FLN B level did not have a statistically significant effect on albumin uptake. Cotransfection of siRNA for FLN A and Cav-1 did not have an additive effect (reduced albumin uptake by 47%), suggesting that FLN A and Cav-1 participate in a common pathway of albumin internalization. Disruption of the actin cytoskeleton by latrinculin B treatment induced cell rounding and decreased BSA uptake by 70%.

To confirm the notion that BSA is internalized primarily via caveolae in endothelial cells and thus can be used as cargo to specifically label caveolae, we purified endothelial cells from lung microvessels of wild-type and *Cav-1*$^{-/-}$ mice and incubated the cells with the Alexa-488-BSA. Whereas caveolin-1–positive cells from wild-type mice internalized a significant amount of albumin, cells purified from *Cav-1*$^{-/-}$ mice showed significantly reduced BSA uptake (Figure 2D). These data suggest that incomplete inhibition of albumin

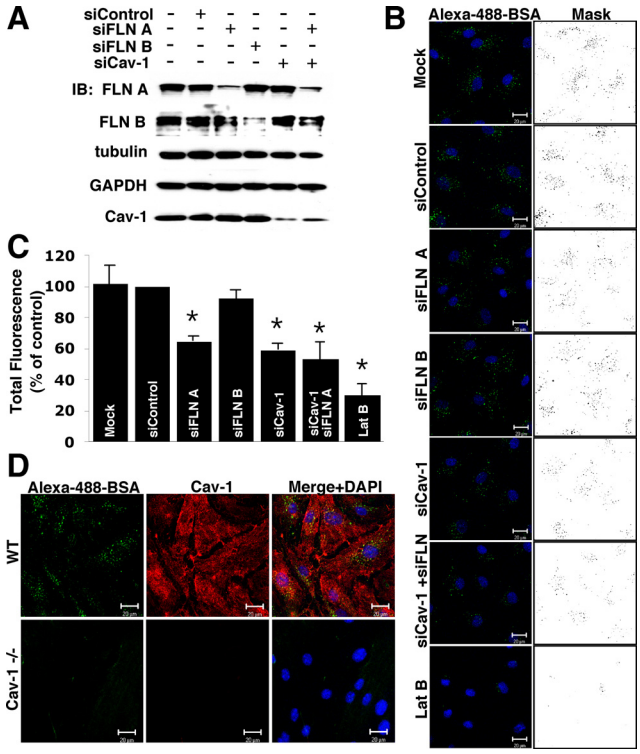

Figure 2. Inhibition of caveolae-mediated endocytosis upon FLN A depletion. (A) HLMVECs were transfected with control, FLN A, FLN B, Cav-1, or a mixture of Cav-1 and FLN A siRNA, and the level of knockdown was examined 72 h after transfection. Western blot analysis confirmed that siRNA-mediated knockdown of FLN A, FLN B and Cav-1 was efficient and selective (see Supplemental Figure S1 for averaged data). (B) HLMVECs transfected with control, FLN A, FLN B, or Cav-1 siRNA alone, a mixture of FLN A and Cav-1 siRNA, or pretreatment with LatB (25 nM for 20 min) were incubated with Alexa-488-BSA (10 μg/ml) for 30 min and acid washed to remove cell surface-associated tracer albumin. Nuclei were stained with DAPI (blue). Images and masks of thresholded images are representative of three independent experiments. Bars, 20 μm. (C) Uptake of Alexa-488-BSA was quantified from thresholded images; the bar graph represents uptake as a percentage of BSA internalized by control siRNA-transfected cells (mean $\pm$ SEM; n = 3). Cells transfected with FLN A, Cav-1 and mixture of FLN A and Cav-1 siRNA showed 35%, 41 and 47% reduction in albumin uptake respectively in comparison with cells transfected with control siRNA ($p < 0.05$). Pretreatment with LatB reduced albumin internalization by 70%, whereas knockdown of FLN B did not induce statistically significant changes in BSA-uptake. (D) Endothelial cells purified from the lungs of wild type and *Cav-1*$^{-/-}$ mice were incubated with Alexa-488-BSA (10 μg/ml) for 30 min; acid washed; and then fixed, permeabilized, and stained for Cav-1. Cells from *Cav-1*$^{-/-}$ mice exhibited significantly reduced albumin uptake, suggesting caveolae-mediated uptake is the primary route of albumin internalization in endothelial cells.

uptake in HLMVECs transfected with Cav-1 siRNA is mainly due to the incomplete knockdown of Cav-1.

Knockdown of Filamin A Reduces Caveolae-mediated Transcytosis of Albumin

Next, we studied the effect of the FLN A knockdown on caveolae-mediated transcytosis. ^{125}I-Albumin was added to the upper chamber of Transwell filter insets in the absence and presence of excess unlabeled albumin, and then radioactivity was measured in aliquots collected from the lower chamber over time (Figure 3A). Note inhibition of total ^{125}I-albumin transport and absence of effect of siRNA on paracellular ^{125}I-albumin permeability (Figure 3B). Transcellular ^{125}I-albumin permeability was calculated as the specific displaceable fraction of ^{125}I-albumin transport per minute per square centimeter (Figure 3C). The rate of transport in cells transfected with control siRNA was 134.4 $\pm$ 19.7 nl/min/cm^2. Knockdown of filamin A reduced albumin permeability by 55%, whereas transfection with FLN B siRNA if anything slightly increased the rate of albumin transport via the transcellular route. Knockdown of Cav-1 alone reduced albumin permeability by 45%, and knockdown of both Cav-1 and FLN A at the same time decreased the rate of albumin transport by 55%, which was not statistically different from that achieved by either siRNA alone. This result, as well as the absence of an additive effect of Cav-1 and FLN A knockdown on albumin uptake, suggests that FLN A specifically participates in caveolae-mediated transport. As with albumin internalization, transfection of Cav-1 siRNA only partially blocked the transendothelial transport of ^{125}I-albumin due to incomplete knockdown of Cav-1. The remaining albumin transport in FLN A or Cav-1 siRNA-transfected cells was not due to leakage through the paracellular pathway because excess unlabeled BSA (100 mg/ml), which only competes with tracer albumin transport via the vesicular pathway (John *et al*., 2003), blocked ^{125}I-albumin transport by >80% (Figure 3B). Furthermore, immunofluorescent staining of VE-cadherin confirmed that adherens junctions remained intact after knockdown of FLN A or FLN B and in fact it was not different from that in control cells (Figure 3D). Thus, siRNA-mediated knockdown of FLN A, but not FLN B, reduced transcellular transport of albumin without affecting paracellular permeability.

Reduction in Filamin A Did Not Affect F/G-Actin Ratio or Stress Fiber Formation

The main function of FLN A is to cross-link actin filaments. To test whether the decrease in caveolae-mediated endocytosis or transcytosis was due to global changes in the actin cytoskeleton, we examined the F/G-actin ratio and stress fiber formation after knockdown of FLN A or FLN B by siRNA.

The amount of F- and G-actin detected in Western blots was quantified by densitometry. Knockdown of FLN A or FLN B did not affect the F/G-actin ratio compared with cells transfected with control siRNA (Supplemental Figure S2A). Jasplakinolide, an actin stress fiber-stabilizing drug, predictably increased the F/G-actin ratio, whereas latrinculin B, which is known to depolymerize actin filaments, significantly decreased the F/G-ratio (Supplemental Figure S2A).

To analyze the amount and localization of polymerized actin, HLMVECs were cotransfected with actin-YFP and either control, FLN A, or FLN B siRNA. No significant difference in actin-YFP staining was detected in cells with reduced FLN A or FLN B expression in comparison with control cells (Supplemental Figure S2B). Staining of siRNA transfected cells with Alexa 568-phalloidin also did not reveal any differences in the structure of the actin cytoskeleton (Supplemental Figure S2B). Thus, we can conclude that the observed reduction in efficiency of caveolae-mediated albumin transport was not due to global changes in the actin cytoskeleton.

siRNA-mediated Knockdown of Filamin A Reduced the Rate of Cav-1-GFP FRAP

HLMVEC were cotransfected with Cav-1-GFP and control siRNA or FLN A siRNA. Seventy-two hours after transfection, cells expressing Cav-1-GFP were subjected to FRAP

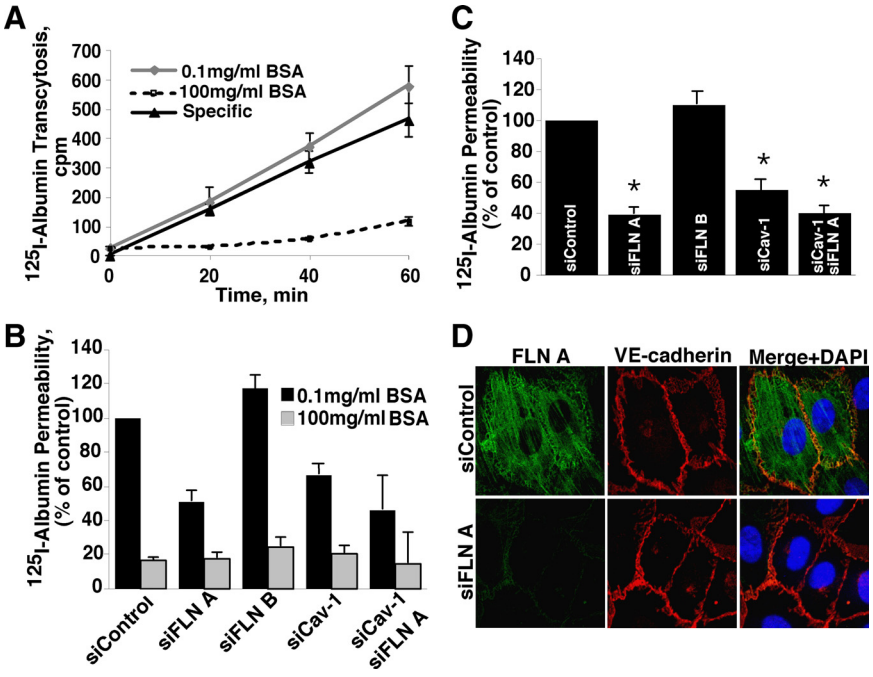

Figure 3. Effect of FLN A, FLN B, and Cav-1 knockdown on transendothelial ^{125}I-albumin transport. (A) HLMVECs grown on Transwell filter inserts were transfected with siRNA. The line graphs show the time course of ^{125}I-BSA transcellular transport through control siRNA-transfected cell monolayers in the presence of 0.1 mg/ml unlabeled BSA (total transport) or 100 mg/ml unlabeled BSA (which measures the nonspecific paracellular leakage of ^{125}I-BSA). Specific vesicular transport of ^{125}I-BSA was obtained by subtraction of the paracellular leakage from total ^{125}I-albumin transport (mean ± SEM; n = 3). (B) Bar graph depicts the normalized total and paracellular ^{125}I-BSA permeability values (mean ± SEM; n = 3) of HLMVEC monolayers obtained in the presence of 0.1 or 100 mg/ml unlabeled BSA. The permeability of monolayers transfected with FLN A, FLN B, Cav-1 or a mixture of FLN A and Cav-1 siRNA is plotted as a % of that observed in cells transfected with control siRNA. Knockdown of FLN A, FLN B or Cav-1 did not affect paracellular ^{125}I-BSA permeability suggesting that integrity of monolayers was not affected by siRNA transfection. (C) Knockdown of FLN A and Cav-1 decreased transcellular albumin permeability by 60 and 50%, respectively compared with cells transfected with control siRNA (mean of 3 independent experiments ± SEM; *$p < 0.05$). Knockdown of both FLN A and Cav-1 did not induce a further reduction in albumin permeability. Transendothelial albumin permeability of cells transfected with FLN B siRNA was not statistically different from that of control siRNA transfected cells. (D) Cells transfected with FLN A or control siRNA were stained with filamin A and VE-cadherin antibodies. Confocal images show that siRNA-mediated knockdown of FLN A did not affect VE-cadherin localization or relative abundance.

analysis. Cells with reduced FLN A protein level showed a delayed recovery of fluorescence in comparison with the cells cotransfected with control siRNA (Figure 4, A and B). The rate of recovery, calculated from the linear portion of the recovery curve immediately after photobleaching, was 1.38×10^{-3} (relative intensity per second) for cells transfected with control siRNA and 0.83×10^{-3} for the cells transfected with FLN A siRNA, which is a 40% reduction in

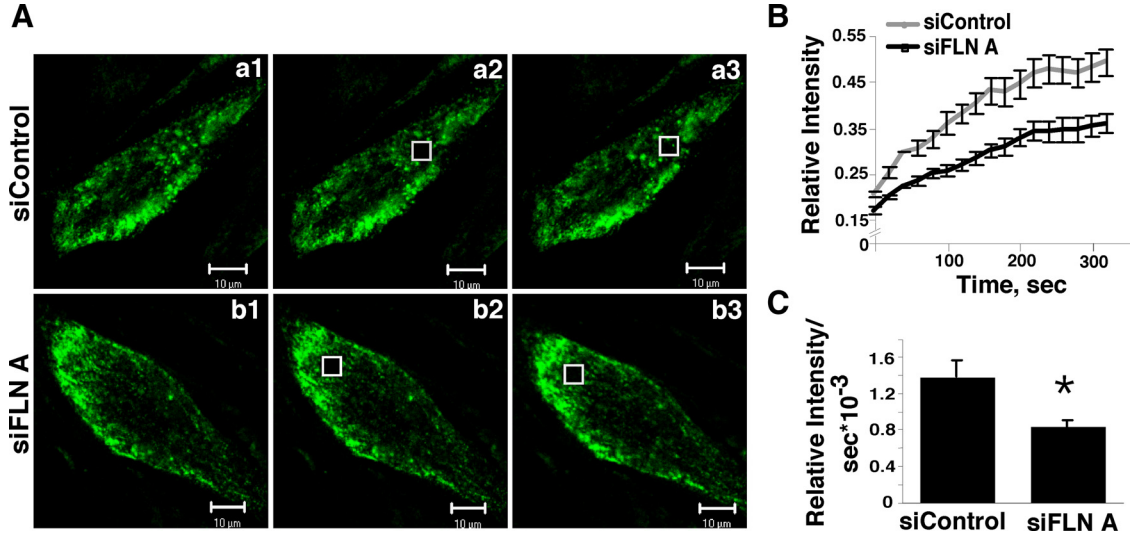

Figure 4. FRAP analysis of Cav-1-GFP mobility in FLN A-depleted HLMVECs. (A) Analysis of Cav-1-GFP confocal images in cells treated with control siRNA (a1–a3) or FLN A siRNA (b1–b3) before photobleaching (a1 and b1), immediately after photobleaching (a2 and b2), and 1.33 min after photobleaching (a3 and b3) suggests that recovery of the Cav-1-GFP signal in the bleached area is delayed in cells in which FLN A has been depleted. Bars, 10 μm. (B) Fluorescence recovery time course calculated from six cells from each of three independent transfections with control versus FLN A siRNA (mean ± SEM; n = 18) shows significantly reduced Cav-1-GFP FRAP in FLN A siRNA-treated cells. (C) The rate of fluorescence recovery was calculated from the linear region of the recovery curve immediately after photobleaching. Cells transfected with FLN A siRNA showed a 40% decrease in the rate of recovery of Cav-1-GFP fluorescence compared with cells transfected with control siRNA (*$p < 0.05$).

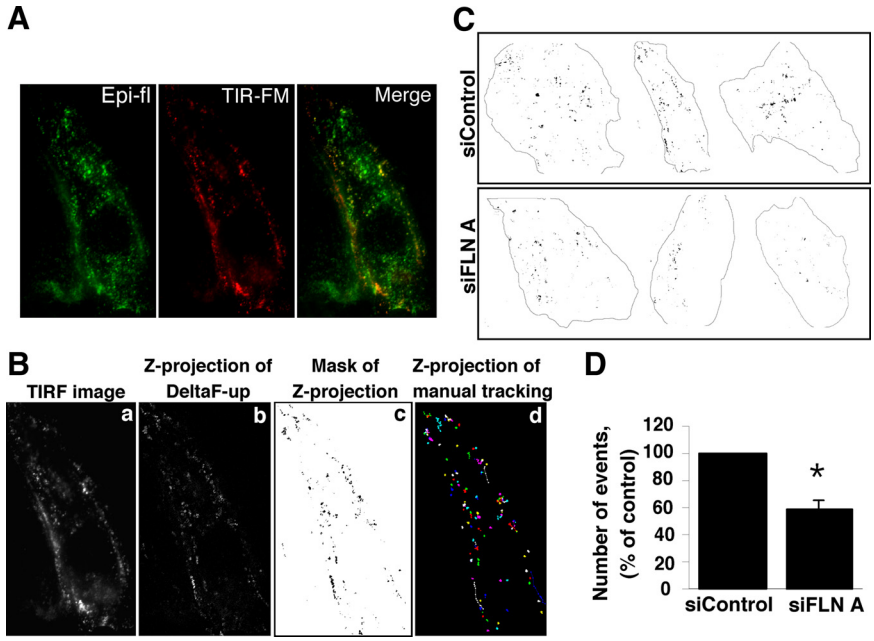

Figure 5. Analysis of Cav-1-GFP mobility by TIR-FM. (A) Comparison of epifluorescent (green) and TIR-FM (red) images of Cav-1-GFP in HLMVECs. (B) Time-series images obtained by TIR-FM were used to generate projections of the changes in Cav-1-GFP localization in or near the membrane over time. Cav-1-GFP membrane mobility includes lateral migration of vesicles, appearance and disappearance of Cav-1-GFP in the TIRF plane due to vesicle fission from and fusion with the plasma membrane, and separation of preexisting vesicle complexes. A single TIRF image is shown in a. Dynamic changes in the TIRF plane were estimated by subtracting each frame from the next using the Delta-F-up ImageJ module. The Z-projection over time of 29 resultant TIRF frames is presented in b. Mask of thresholded Z-projection is shown in c. Z-projection of 115 manually tracked vesicles is presented in d. Tracks observed by manual tracking were identical to those obtained with ImageJ software. (C) Three examples of Cav-1-GFP projection masks in control siRNA and FLN A siRNA-treated cells are shown. (D) Bar graph represents the total number of mobile Cav-1–GFP-labeled vesicle movements per unit area as a percentage of events registered in cells transfected with control siRNA (mean ± SEM). The overall mobility of Cav-1-GFP was reduced in FLN A siRNA-transfected cells by 41.4 ± 6.9% ($p = 0.0052$).

the rate of movement of Cav-1–GFP-labeled intracellular structures in cells with reduced FLN A expression ($p < 0.05$ vs. control; Figure 4C). This result suggests that FLN A plays an important role in caveolae trafficking.

Mobility of Cav-1-GFP at the Membrane Is Reduced in Cells Transfected with Filamin A siRNA

To analyze the role of FLN A in Cav-1–enriched vesicle membrane dynamics, HLMVECs were cotransfected with Cav-1-GFP and control or FLN A siRNA and subjected to live-cell TIR-FM. The Cav-1-GFP signal in the TIRF plane of HLMVECs was primarily concentrated at the cell borders in large clusters of vesicles, whereas more punctuate and vesicular Cav-1-GFP staining was detected in central regions of the cells (Figure 5A). Cav-1–GFP-labeled vesicles were heterogeneous in size and showed several different patterns of behavior. The majority of vesicles were stable and did not move throughout the time course of the experiment or showed oscillating low-range movements. We also detected vesicles that appeared and disappeared in the TIRF plane due to transient association and dissociation with the plasma membrane; presumably these objects represent the fission and fusion of preexisting vesicles. A small number of vesicles, usually one to five per cell, showed very fast directional movement. Because of the complexities of Cav-1-GFP dynamics in or near the plasma membrane, we estimated changes in Cav-1-GFP over 30 frames by subtracting subsequent frames to create a projection of the changes in Cav-1-GFP over time (Figure 5, B and C). The number of events observed in cells transfected with FLN A siRNA, thus representative of the changes in Cav-1-GFP localization due to movement within the TIRF plane, was calculated from thresholded projections and expressed as a percentage of the number of Cav-1-GFP events detected in cells treated with control siRNA (Figure 5D). The mobility of Cav-1–GFP-labeled vesicles was reduced by 41% ($p < 0.05$ vs. control siRNA; Figure 5D) in cells transfected with FLN A siRNA, further suggesting that FLN A regulates the membrane dynamics of caveolae.

Comparative Analysis of Cav-1-GFP Distribution in M2 and A7 Cells

M2 cells that do not express endogenous FLN A and A7 cells in which FLN A expression was restored have the same level of FLN B and actin as shown by Western blot analysis (Figure 6A). Surprisingly, a very small amount of caveolin-1 was observed in A7 cells but not observed in M2 cells. However, the level of exogenously expressed GFP-tagged Cav-1 in M2 and A7 cells was several-fold higher than the level of endogenous Cav-1 observed in A7 cells; thus, it was not considered further (Figure 6A). Using this model system, Cav-1 distribution in the presence and absence of FLN A (i.e., M2 and A7 cells transfected with Cav-1-GFP) was observed in fixed cells 24 h after transfection. In A7 cells, Cav-1-GFP was concentrated in large vesicles located primarily in the cytoplasmic compartment (Figure 6Ba and 6Ca1), whereas in M2 cells, we detected diffuse Cav-1-GFP labeling of the plasma membrane and less vesicular staining (Figure 6Bd and 6Cb1). Cotransfection of M2 cells with Cav-1-GFP and FLN A-RFP to acutely rescue FLN A expression showed that the majority of Cav-1-GFP was localized to large vesicular structures (Figure 6Bg and Figure 6Cc1), confirming the phenotype observed in the FLN A-positive A7 cells that FLN A regulates the organization and trafficking caveolin-1–labeled vesicles.

In both cell lines, Cav-1-GFP was found associated with large intracellular vesicles and partially colocalized with internalized Alexa-546 CTB (Supplemental Figure S3A) and a marker of early endosomes, EEA1 (Supplemental Figure S3B), but not with lysosomal marker lysosome-associated membrane protein-1 (Lamp-1) (Supplemental Figure S3C). Orthogonal projection images showing X-Z profiles of M2 and A7 cells expressing Cav-1-GFP that were stained for FLN A and M2 cells cotransfected with Cav-1-GFP and FLN A-RFP confirmed that in the presence of FLN A, Cav-1 is organized into large vesicular structures that are located in the cytoplasm (Figure 6C, a1 and c1). In M2 cells lacking

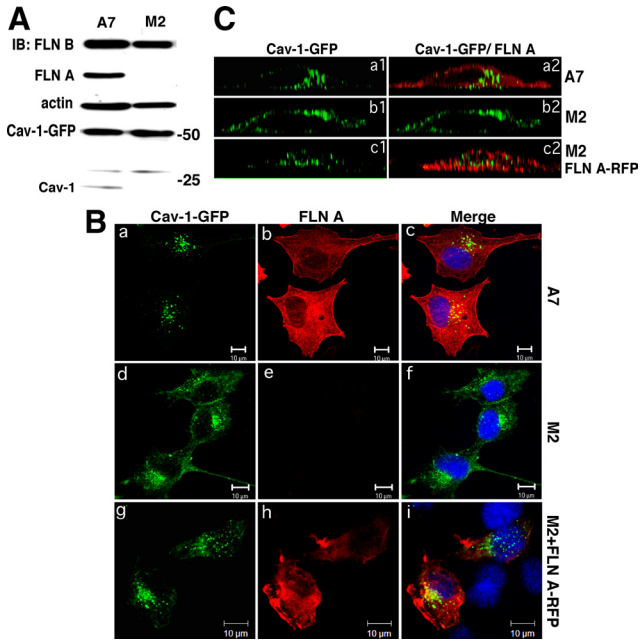

Figure 6. Cav-1-GFP distribution in M2 and A7 cells. (A) Western Blot analysis of M2 and A7 cell lysates confirmed expression of FLN A in A7 cells and the lack of FLN A in M2 cells. The level of expression of FLN B and actin was similar in both cell lines. In A7 cells, endogenous Cav-1 expression was also observed, albeit ~10-times lower than the level of Cav-1-GFP. (B) M2 (a, b, c, g, h, and i) and A7 cells (d–f) were transfected with Cav-1-GFP alone (a and d) or cotransfected with FLN A-RFP (g–i), fixed 24 h after transfection, and stained with FLN A mAb (b, e, and h). Merged images also show DAPI nuclear staining (c, f, and i). Bars, 10 μm. Cav-1-GFP distribution was more punctate and internalized in A7 cells and M2 cells cotransfected with FLN A-RFP and diffusely membrane-associated in M2 cells. (C) Z-axis deconvolved orthogonal projection images of A7 (a1 and a2) and M2 (b1, b2, c1, and c2) cells transfected with Cav-1-GFP (b1 and b2) or cotransfected with Cav-1-GFP and FLN A-RFP (c1 and c2). Merged images show Cav-1-GFP and FLN A staining (a2, b2, and c2). A7 cells and M2 cells expressing FLN A-RFP showed clustered and internalized Cav-1-GFP, whereas in M2 cells Cav-1 was localized to the plasma membrane.

FLN A, Cav-1 was evenly distributed over the plasma membrane (Figure 6Cb1).

DISCUSSION

In the present study, we demonstrate that FLN A, but not FLN B, associates with Cav-1 in endothelial cells. We also observed that the full C terminus of FLN A is sufficient for binding Cav-1 in vivo, which goes along with in vitro data obtained by others (Stahlut and van Deurs, 2000). Furthermore, we showed that FLN A partially colocalizes with Cav-1, Cav-2, c-Src, and dynamin-2 in cholesterol-enriched density gradient fractions. We observed that Src activation via stimulation of albumin-binding protein gp60 (Tiruppathi *et al.*, 1997; Minshall *et al.*, 2000) and/or phosphatase inhibition with sodium orthovanadate (Shajahan *et al.*, 2004a,b) induced a shift of both FLN A and actin to buoyant fractions of the gradient, leading to the enhanced cofractionation of FLN A and Cav-1. Under these conditions, we observed greater Cav-1 coimmunoprecipitation with FLN A compared with serum-deprived cells. On the contrary, cells pretreated with Src-family kinase inhibitor PP2 showed reduced amounts of FLN A and actin in buoyant fractions of the gradient, as well as the amount of Cav-1 that coprecipitated with FLN A. Thus, we propose that FLN A associates with caveolin-1 in endothelial cells and is actively recruited to albumin-loaded and activated caveolae. We (Tiruppathi *et al.*, 1997; Minshall *et al.*, 2000; Shajahan *et al.*, 2004a,b; Hu *et al.*, 2006; Hu *et al.*, 2008b) and others (Sharma *et al.*, 2004) have previously shown that activation of Src family kinases is a critical step in the process of caveolae-mediated endocytosis (for review, see Sverdlov *et al.*, 2007). The data provided in the present study suggest that Src facilitates interactions between caveolae and the actin cytoskeleton by enhancing the association between Cav-1 and FLN A.

A recent study suggested that FLN A and Cav-1 interact not at the plasma membrane but rather in the cytoplasm (Ravid *et al.*, 2008a). However, Stahlut and van Deurs (2000) demonstrated by both fluorescence and electron microscopy that filamin colocalizes with Cav-1 at the plasma membrane in proximity to caveolae. Our data indicate that this interaction takes place in the membrane in endothelial cells as well.

Both Cav-1 and FLN A are highly expressed in endothelial cells. However, only a small fraction of each of these proteins can be found in association. There may be several explanations for this. First, Cav-1–FLN A interactions probably are phosphorylation-dependent and thus transient. Second, regulation of caveolae-mediated endocytosis and trafficking is only one of the functions of FLN A. Finally, FLN A probably interacts only with the subset of caveolae that are actively engaged in caveolae-mediated endocytosis and transcytosis.

To assess the function of FLN A in caveolae-mediated transport, we knocked down FLN A in HLMVECs and analyzed the extent and dynamics of caveolae-mediated albumin endocytosis and transcytosis. Albumin uptake and transendothelial permeability via caveolae were reduced by ~35 and 60%, respectively, in cells transfected with FLN A siRNA, suggesting that FLN A is necessary for efficient caveolae internalization and trafficking. Furthermore, siRNA-mediated double knockdown of FLN A and Cav-1 did not further reduce albumin uptake or permeability, implying that FLN A and Cav-1 participate in a common endocytic mechanism. siRNA-mediated knockdown of the FLN A homologue FLN B did not significantly affect caveolae-mediated uptake or transport.

FLN A knockout mice are embryonically lethal, which may be due in part to vascular defects including VE-cadherin mislocalization resulting in vascular leakage (Feng *et al.*, 2006). Our studies revealed that in cells transfected with either FLN A or FLN B siRNA, VE-cadherin localization was not different from that of control cells (Figure 3D), implying that the residual amount of FLN A was sufficient for proper VE-cadherin localization. Furthermore, our data support the contention that knockdown of FLN A or FLN B did not disrupt endothelial cell monolayer integrity in that excess unlabeled albumin (100 mg/ml) was still able to block ^{125}I-BSA transport in HLMVEC monolayers, which would only be possible if the monolayer was not leaky, i.e., if caveolae mediated the bulk of the transcellular transport. From these studies, we can conclude that siRNA-mediated reduction in FLN A expression decreased transcellular albumin transport without affecting the junctional permeability pathway.

It is believed that the main function of FLN A in cells is to organize the actin cytoskeleton. Because it was shown previously that the actin cytoskeleton is crucial for caveolae-mediated endocytosis (Parton *et al.*, 1994; Mundy *et al.*, 2002; Pelkmans *et al.*, 2002), we tested whether the decrease in caveolae-mediated endocytosis and transcytosis in FLN A

siRNA-transfected cells was due to global changes in actin cytoskeletal networks. We demonstrated that there were no significant differences in the F/G-actin ratio or localization pattern in cells transfected with control, FLN A or FLN B siRNA. Consistent with our observation, a previous report indicated that fibroblasts, neurons, and endothelial cells derived from FLN A knockout mouse embryos had stress fibers, a cortical actin band, and focal adhesions that were indistinguishable from that of cells from wild-type embryos (Feng *et al*., 2006). Thus, the reduction in caveolae-mediated albumin uptake and transcytosis is unlikely to be due to alterations in the general framework of the actin cytoskeleton. However, this does not exclude the possibility that cells transfected with FLN A siRNA may be defective with respect to the regulation of local transient actin remodeling induced upon stimulation of caveolae formation and/or activation of endocytosis and transcytosis.

Because our data indicate that siRNA-mediated knockdown of FLN A is associated with a modest reduction (30%) in albumin endocytosis but a nearly 60% decrease in transendothelial albumin permeability, we measured the mobility of caveolae by FRAP after FLN A knockdown. Thomsen *et al*. (2002) showed by FRAP analysis that plasma membrane-associated Cav-1-GFP was relatively immobile in comparison with the fast-moving intracellular pool of GFP-labeled Cav-1. Based on these data, we monitored the recovery of Cav-1-GFP fluorescence from a small area within cells transfected with either control or FLN A siRNA. Knockdown of FLN A induced a 40% reduction in the fluorescence recovery rate of Cav-1-GFP compared with cells transfected with control siRNA, implying a significantly slower migration of GFP-labeled vesicles in the cells with reduced FLN A expression.

We also measured the dynamics of Cav-1–GFP-labeled vesicles at the membrane by TIR-FM in which fluorophore excitation is limited to ~100 nm beyond the coverslip. TIR-FM showed that the majority of vesicles were stable throughout the experiment, which is in agreement with previous TIR-FM studies of caveolae (Pelkmans and Zerial, 2005; Tagawa *et al*., 2005). However, we also observed vesicles undergoing fission and fusion events at the plasma membrane and with Cav-1–GFP-labeled membranes. Finally, a very small number of vesicles were actively engaged in very fast directional movement. In FLN A siRNA-treated cells, the mobility of Cav-1-GFP at the membrane was significantly reduced compared with control siRNA-treated cells.

To better understand the functional role of FLN A in caveolae-mediated transport, we also studied the distribution of Cav-1-GFP in M2 cells that lack endogenous FLN A and in A7 cells in which FLN A expression had been restored. In the absence of FLN A, Cav-1-GFP was evenly distributed over the plasma membrane and to a much lesser extent, associated with intracellular vesicular structures. In A7 cells, however, the majority of Cav-1-GFP was organized into large vesicles localized primarily in the cytosolic compartment. Importantly, cotransfection of Cav-1-GFP and FLN A-RFP to acutely rescue both Cav-1 and FLN A in M2 cells was associated with enhanced formation of large cytoplasmically localized vesicles. In both the M2 and A7 cell lines, intracellular Cav-1-GFP labeling was mobile and partially colocalized with early endosomal marker EEA1 but not with lysosomal marker Lamp-1. Neither M2 nor A7 cells transfected with Cav-1-GFP were able to internalize albumin, perhaps due to the lack of specific albumin-binding protein gp60 in caveolae but did in fact take up cholera toxin subunit B, which colocalized with Cav-1-GFP in both M2 and A7 cells. However, because CTB uptake was not specific to Cav-1–GFP-labeled vesicles, the extent and localization of CTB uptake was not different between the two cell lines.

FLN A participates in the organization and internalization of caveolae, although the mechanism is not clear. One possibility is that FLN A, through an association with the actin cytoskeleton, spatially organizes caveolae and also facilitates caveolae clustering. It may also be that FLN A facilitates caveolae-mediated transport by regulating localized cytoskeletal actin dynamics. FLN A was previously shown to bind several small GTPases, however, only RalA was shown to bind to FLN A in its active GTP-bound form (Yasutaka *et al*., 1999). Moreover, Cav-1 and RalA bind adjacent C-teminal domains of FLN A (Yasutaka *et al*., 1999; Stahlut and van Deurs, 2000). Because RalA was previously shown to participate in Src activation and regulation of clathrin-mediated endocytosis, membrane trafficking, and formation of exocyst complexes (Feig, 2003), it is interesting to speculate that RalA may participate in FLN A-dependent regulation of caveolae-mediated endocytosis and transcytosis.

ACKNOWLEDGMENTS

We thank Dr. Mei-ling Chen in Research Resources Center Imaging facility for assistance with TIR-FM experiments and Drs. Oleg Chaga and Tiffany Sharma in the Department of Pharmacology Imaging Facility and Molecular Resources Core, respectively, for excellent support. We gratefully acknowledge Drs. F. Nakamura, W. H. Ziegler, and D. Mehta for providing valuable reagents as specified in Methods. We also thank Dr. Randal A. Skidgel and Dr. Dolly Mehta (University of Illinois at Chicago) and Dr. Geerten van Nieuw Amerongen (Vrije University Medical Center, Amsterdam, The Netherlands) for their thoughtful discussions. This work was supported by National Institutes of Health, National Heart, Lung and Blood Institute grants P01 HL60678, R01 HL71626, T32 HL072742, and S10 RR022547-01A1 from the National Center for Research Resources which funded the TIR-FM system. This manuscript is based upon a thesis in partial fulfillment of the requirements for the doctoral degree at the Graduate College of the University of Illinois at Chicago.

REFERENCES

Beekman, J. M., van der Poel, C. E., van der Linden, J. A., van den Berg, D.L.C., van den Berghe, P.V.E., van de Winkel, J.G.J., and Leusen, J.H.W. (2008). Filamin A stabilizes FcγRI surface expression and prevents its lysosomal routing. J. Immunol. *180*, 3938–3945.

Doucey, M.-A., Bender, F. C., Hess, D., Hofsteenge, J., and Bron, C. (2006). Caveolin-1 interacts with the chaperone complex TCP-1 and modulates its protein folding activity. Cell Mol. Life Sci. 1–10.

Feig, L. A. (2003). Ral-GTPases: approaching their 15 minutes of fame. Trends Cell Biol. *13*, 419–425.

Feng, Y., Chen, M. H., Moskowitz, I. P., Mendonza, A. M., Vidali, L., Nakamura, F., Kwiatkowski, D. J., and Walsh, C. A. (2006). Filamin A (FLNA) is required for cell-cell contact in vascular development and cardiac morphogenesis. Proc. Natl. Acad. Sci. USA *103*, 19836–19841.

Head, B. P., Patel, H. H., Roth, D. M., Murray, F., Swaney, J. S., Niesman, I. R., Farquhar, M. G., and Insel, P. A. (2006). Microtubules and actin microfilaments regulate lipid raft/caveolae localization of adenylyl cyclase signaling components. J. Biol. Chem. *281*, 26391–26399.

Hu, G., Schwartz, D. E., Shajahan, A. N., Visintine, D. J., Salem, M. R., Crystal, G. J., Albrecht, R. F., Vogel, S. M., and Minshall, R. D. (2006). Isoflurane, but not sevoflurane, increases transendothelial albumin permeability in the isolated rat lung. Anesthesiology *104*, 777–785.

Hu, G., Place, A. T., and Minshall, R. D. (2008a). Regulation of endothelial permeability by Src kinase signaling: vascular leakage versus transcellular transport of drugs and macromolecules. Chem. Biol. Interact. *171*, 177–189.

Hu, G., Vogel, S. M., Schwartz, D. E., Malik, A. B., and Minshall, R. D. (2008b). Intercellular adhesion molecule-1-dependent neutrophil adhesion to endothelial cells induces caveolae-mediated pulmonary vascular hyperpermeability. Circ. Res. *102*, 120–131.

Izumi, T., Shibata, Y., and Yamamoto, T. (1991). Quick-freeze, deep-etch studies of endothelial components, with special reference to cytoskeletons and vesicle structures. J. Electron Microsc. *19*, 316–326.

John, T. A., Vogel, S. M., Tiruppathi, C., Malik, A. B., and Minshall, R. D. (2003). Quantitative analysis of albumin uptake and transport in the rat microvessel endothelial monolayer. Am. J. Physiol. Lung Cell Mol. Physiol. *284*, L187–L196.

Krueger, E. W., Orth, J. D., Cao, H., and McNiven, M. A. (2003). A dynamin-cortactin-Arp2/3 complex mediates actin reorganization in growth factor-stimulated cells. Mol. Biol. Cell *14*, 1085–1096.

Lee, E., and Camilli, P. D. (2002). Dynamin at actin tails. Proc. Natl. Acad. Sci. USA *99*, 161–166.

Macdonald, J. L., and Pike, L. J. (2005). A simplified method for the preparation of detergent-free lipid rafts. J. Lipid Res. *46*, 1061–1067.

McNiven, M. A., Kim, L., Krueger, E., Orth, J. D., Cao, H., and Wong, T. W. (2000). Regulated interactions between dynamin and the actin-binding protein cortactin modulate cell shape. J. Cell Biol. *151*, 187–198.

Minshall, R. D., and Malik, A. B. (2006). Transport across the endothelium: regulation of endothelial permeability. In: Handbook of Experimental Pharmacology, Vol. 176, ed. S. Moncada and A. Higgs, Heidelberg, Germany: Springer-Verlag, 107–144.

Minshall, R. D., Sessa, W. C., Stan, R. V., Anderson, R.G.W., and Malik, A. B. (2003). Caveolin regulation of endothelial function. Am. J. Physiol. Lung Cell Mol. Physiol. *285*, L1179–L1183.

Minshall, R. D., Tiruppathi, C., Vogel, S. M., Niles, W. D., Gilchrist, A., Hamm, H. E., and Malik, A. B. (2000). Endothelial cell-surface gp60 activates vesicle formation and trafficking via Gi-coupled Src kinase signaling pathway. J. Cell Biol. *150*, 1057–1069.

Morone, N., Fujiwara, T., Murase, K., Kasai, R. S., Ike, H., Yuasa, S., Usukura, J., and Kusumi, A. (2006). Three-dimensional reconstruction of the membrane skeleton at the plasma membrane interface by electron tomography. J. Cell Biol. *174*, 851–862.

Mundy, D. I., Machleidt, T., Ying, Y.-S., Anderson, R.G.W., and Bloom, G. S. (2002). Dual control of caveolar membrane traffic by microtubules and the actin cytoskeleton. J. Cell Sci. *115*, 4327–4339.

Onoprishvili, I., Andria, M. L., Kramer, H. K., Ancevska-Taneva, N., Hiller, J. M., and Simon, E. J. (2003). Interaction between the μ opioid receptor and filamin A is involved in receptor regulation and trafficking. Mol. Pharmacol. *64*, 1092–1100.

Orth, J. D., Krueger, E. W., Cao, H., and McNiven, M. A. (2002). The large GTPase dynamin regulates actin comet formation and movement in living cells. Proc. Natl. Acad. Sci. USA *99*, 167–172.

Parton, R. G., Joggerst, B., and Simons, K. (1994). Regulated internalization of caveolae. J. Cell Biol. *127*, 1199–1215.

Parkar, N. S., Akba, B. S., Nitsche, L. C., Wedgewood, L. E., Sverdlov, M. S., Place, A. T., Chaga, O., and Minshall, R. D. (2009). Vesicle formation and endocytosis: function, machinery, mechanisms, and modeling. Antioxid. Redox Signal. *11*, 1301–1312.

Pelkmans, L., and Helenius, A. (2002). Endocytosis via caveolae. Traffic *3*, 311–320.

Pelkmans, L., Püntener, D., and Helenius, A. (2002). Local actin polymerization and dynamin recruitment in SV40-induced internalization of caveolae. Science *296*, 535–539.

Pelkmans, L., and Zerial, M. (2005). Kinase-regulated quantal assemblies and kiss-and-run recycling of caveolae. Nature *436*, 128–133.

Predescu, S. A., Predescu, D. N., Timblin, B. K., Radu Stan, V., and Malik, A. B. (2003). Intersectin regulates fission and internalization of caveolae in endothelial cells. Mol. Biol. Cell *14*, 4997–5010.

Ravid, D., Chuderland, D., Landsman, L., Lavie, Y., Reich, R., and Liscovitch, M. (2008a). Filamin A is a novel caveolin-1-dependent target in IGF-I-stimulated cancer cell migration. Exp. Cell Res. *314*, 2762–2773.

Ravid, D., Chuderland, D., Landsman, L., Lavie, Y., Reich, R., and Liscovitch, M. (2008b). Filamin A is a novel caveolin-1-dependent target in IGF-I-stimulated cancer cell migration. Exp. Cell Res. *314*, 2762–2773.

Richter, T., Floetenmeyer, M., Ferguson, C., Galea, J., Goh, J., Lindsay, M. R., Morgan, G. P., Marsh, B. J., and Parton, R. G. (2008). High-resolution 3D quantitative analysis of caveolar ultrastructure and caveolae-cytoskeleton interactions. Traffic *9*, 893–909.

Schafer, D. A., Weed, S. A., Binns, D., Karginov, A. V., Parsons, J. T., and Cooper, J. A. (2002). Dynamin 2 and cortactin regulate actin assembly and filament organization. Curr. Biol. *12*, 1852–1857.

Searles, C. D., Ide, L., Davis, M. E., Cai, H., and Weber, M. (2004). Actin cytoskeleton organization and posttranscriptional regulation of endothelial nitric oxide synthase during cell growth. Circ. Res. *95*, 488–495.

Seck, T., Baron, R., and Horne, W. C. (2003). Binding of filamin to the C-terminal tail of the calcitonin receptor controls recycling. J. Biol. Chem. *278*, 10408–10416.

Shajahan, A. N., Timblin, B. K., Sandoval, R., Tiruppathi, C., Malik, A. B., and Minshall, R. D. (2004a). Role of Src-induced dynamin-2 phosphorylation in caveolae-mediated endocytosis in endothelial cells. J. Biol. Chem. *279*, 20392–20400.

Shajahan, A. N., Tiruppathi, C., Smrcka, A. V., Malik, A. B., and Minshall, R. D. (2004b). G$\beta\gamma$ activation of Src induces caveolae-mediated endocytosis in endothelial cells. J. Biol. Chem. *279*, 48055–48062.

Sharma, D. K., Brown, J. C., Choudhury, A., Peterson, T. E., Holicky, E., Marks, D. L., Simari, R., Parton, R. G., and Pagano, R. E. (2004). Selective stimulation of caveloar endocytosis by glycosphingolipids and cholesterol. Mol. Biol. Cell *15*, 3114–3122.

Stahlut, M., and van Deurs, B. (2000). Identification of filamin as a novel ligand for caveolin-1, evidence for the organization of caveolin-1-associated membrane domains by the actin cytoskeleton. Mol. Biol. Cell *11*, 325–337.

Stossel, T. P., Condeelis, J., Cooley, L., Hartwig, J. H., Noegel, A., Schleicher, M., and Shapiro, S. S. (2001). Filamins as integrators of cell mechanics and signalling. Nat. Rev. Mol. Cell Bio. *2*, 138–145.

Sverdlov, M., Shajahan, A. N., and Minshall, R. D. (2007). Tyrosine phosphorylation-dependence of caveolae-mediated endocytosis. J. Cell Mol. Med. *11*, 1239–1250.

Tagawa, A., Mezzacasa, A., Hayer, A., Longatti, A., Pelkmans, L., and Helenius, A. (2005).). Assembly and trafficking of caveolae domains in the cell: caveolae as stable, cargo-triggered vesicular transporters. J. Cell Biol. *170*, 769–779.

Thomsen, P., Roepstorff, K., Stahlut, M., and van Deurs, B. (2002). Caveolae are highly immobile plasma membrane microdomains, which are not involved in constitutive endocytic trafficking. Mol. Biol. Cell *13*, 238–250.

Tiruppathi, C., Song, W., Bergenfeldt, M., Sass, P., and Malik, A. B. (1997). Gp60 activation mediates albumin transcytosis in endothelial cells by tyrosine kinase-dependent pathway. J. Biol. Chem. *272*, 25968–25975.

Ohta, Y., Suzuki, N., Nakamura, S., Hartwig, J. H., and Stossel, T. P. (1999). The small GTPase RalA targets filamin to induce filopodia. Proc. Natl. Acad. Sci. USA *96*, 2122–2128.